INTERNATIONAL JOURNAL FOR NUMERICAL METHODS IN FLUIDS
Int. J. Numer. Meth. Fluids 2001; **35**: 55–70

The hydrodynamic force and torque on a bounded sphere in Poiseuille flow

D. S. Clague[a,b,*,1] and P. J. Cornelius[b,2]

[a] *Center for Computational Engineering/EETD, L-223, Lawrence Livermore National Laboratory, Livermore, CA, U.S.A.*
[b] *Center for Microtechnology/EETD, L-223, Lawrence Livermore National Laboratory, Livermore, CA, U.S.A.*

SUMMARY

The lattice Boltzmann (LB) method is used to study the hydrodynamic force and torque acting on a sphere held stationary between parallel plates in pressure-driven flow. This and associated flow configurations are explored in this paper. LB results are in excellent agreement with existing theory and numerical results for simple pressure-driven flow between parallel plates, for flow through a periodic medium of spheres [Zick AA, Homsy GM. Stokes flow through periodic arrays of spheres. *Journal of Fluid Mechanics* 1982; **115**:13], and for the force and torque acting on a sphere held fixed at the quarter vertical position in a pressure-driven flow between parallel plates. In the latter case, LB calculations reveal a screening effect caused by neighboring periodic images of the test sphere. It is shown that the test sphere is hydrodynamically decoupled from its periodic images when separated by approximately 30 sphere radii. LB results for force and torque as a function of sphere height and flow cell height are also reported. Copyright © 2001 John Wiley & Sons, Ltd.

KEY WORDS: lattice Boltzmann; pressure-driven flow; force and torque

1. INTRODUCTION

Fluid flow over suspended objects in confined domains is of considerable interest in many arenas. The applications range from physiological systems to processing of inks (colloidal systems). Here we are particularly interested in determining the hydrodynamic force and torque acting on a captured spherical particle held fixed between infinite parallel plates in Poiseuille flow. In particular, the purpose of this work was to study the forces and torques acting on spores and macromolecules that have been captured by magnetic and/or electric fields, e.g., external field-induced migration to a bounding surface [2] in flow cells where the

* Correspondence to: Center for Computational Engineering/EETD, L-223, Lawrence Livermore National Laboratory, Livermore, CA 94550, U.S.A.
[1] E-mail: clague@llnl.gov
[2] E-mail: cornelius5@llnl.gov

Received 2 November 1999
Revised 8 March 2000

height of the cell is small compared with the depth and length. Because the suspended species are in a bounded domain, i.e., channel walls are in close proximity, it necessary to accurately account for hydrodynamic wall effects. Notable past approaches used to study particulate media in bounded flows include Wakiya [3], Dabros [4], Durlofsky and Brady [5], and Hu [6].

Wakiya [3] applied Faxen's [7] method to calculate the force and torque acting on a spherical stationary object in flow domains, which included walls. Specifically, Wakiya applied the method of reflections to calculate the force and torque acting on a sphere in Poiseuille and Couette flows. As presented in Happel and Brenner [8], Wakiya's analysis includes two reflections as defined in the method of reflections [8].

Dabros and van de Ven [4], on the other hand, made use of boundary element methods to elucidate the role of particle wall hydrodynamic interactions experienced in colloidal deposition processes. In their work, they explore a few fundamental problems to validate their approach. Specifically, they determine the hydrodynamic force acting on an isolated sphere in a direct, perpendicular approach to a wall. They also explore the drag correction factor for two equal sized spheres aligned in a uniform flow; they note a drag reduction on the sphere pair. A form of the latter problem is explored here.

Durlofsky and Brady [5] developed a singularity method that simultaneously accounts for the bounding walls and inter-particle interactions. In their approach, they represent the wall with interacting wall patches. Therefore, the presence of the wall is built into the grand mobility and resistance matrices in a natural way.

Finally, Hu [6] developed an arbitrary Lagrangian–Eulerian (ALE) Galerkin finite element approach to study cylinders (two-dimensional) and spheres (three-dimensional) in fluids. In his approach, Hu uses a form of adaptive mesh refinement when particles are nearly touching and for when they are in close proximity to the bounding walls. Furthermore, to ensure non-singular behavior at small separations, there is a thin layer of elements always present at each surface. The interested reader is directed to Reference [6] for details.

All of the approaches cited above do indeed take into account wall effects but with varying degrees of difficulty. Here we use the lattice Boltzmann (LB) method [9–12]. The LB method has been successfully applied to a wide variety of physical systems involving particulate media [9–11,13]. In particular, the LB method is uniquely suited for hydrodynamic studies involving particulate media with bounding walls [12,14]. This is primarily due to the ease at which the no-slip condition is enforced at solid surfaces, i.e., the simple bounce back scheme [12,15]. By accounting for the wall surface at the *half* link position between adjacent wall and fluid sites, He and Lou [15] have shown that the LB method captures the boundary condition to nearly second-order accuracy with spatial grid refinement. Therefore, with a sufficient grid refinement, the LB approach is both accurate and extremely flexible. Essentially, in the study of flow through complex media, one is limited only by one's ability to describe the geometric features of the medium, e.g., a core sample of sandstone was imaged and mapped onto a lattice permitting the study of two-phase (oil–water) flow through the semi-permeable medium [9].

The remainder of this paper is separated into five additional sections. In Section 2 the flow configurations studied are presented. Section 3 contains a brief description of the LB method, Section 4 has LB results for pressure driven between infinite parallel plates and for flow through an infinite medium of spheres. In Section 5, LB force and torque calculations are presented for a sphere held fixed in a bi-periodic flow cell. The effects of sphere and simulation cell height are explored. Finally, Section 6 contains the concluding remarks.

2. FLOW CONFIGURATIONS

In the study presented here, we are interested in calculating the force and torque acting on a single, stationary spherical particle positioned at various heights between infinite, parallel plates in Poiseuille flow. To have confidence in the results to follow, it is necessary to demonstrate the LB method on the fundamental problems, i.e., Poiseuille flow between infinite, parallel plates and flow through a periodic array of spheres, which make up the system of interest. With this foundation, we can calculate with confidence the force and torque acting on a particle held fixed between parallel plates.

2.1. Fundamental flow configurations

The first fundamental problem is simply pressure-driven flow of a viscous fluid between infinite, parallel plates. Because we are interested in the force and torque acting on stationary spherical particles in this flow configuration, it is necessary to quantify the error between the LB method and exact theory for Poiseuille flow between parallel plates. For flow through such a cell, the exact solution for the velocity field is

$$u_1(x_3) = -\frac{\Delta P}{2\mu}(x_3 H - x_3^2) \tag{1}$$

Here, $u_{x_1}(x_3)$ is the x_1 component of fluid velocity, which is a function of x_3, the vertical direction in the flow cell, as shown in Figure 1. H is the vertical gap between bounding walls. ΔP is the pressure drop, and μ is the fluid viscosity. The pressure drop in the x_1-direction induces an associated fluid velocity, U.

The next fundamental flow problem is for low-Reynolds number flow of a viscous fluid through a periodic array of spheres (see Figure 2). For this particular flow configuration, the quantity of interest is the hydrodynamic drag force acting on the central sphere. LB results are compared with the well-accepted numerical results of Zick and Homsy [1] in Section 4.

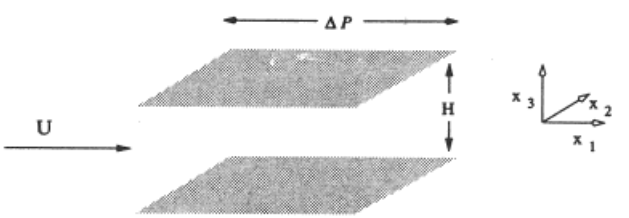

Figure 1. Poiseuille flow between parallel plates. Viscous fluid is forced through the gap, H, between the infinite parallel plates by the pressure drop, ΔP.

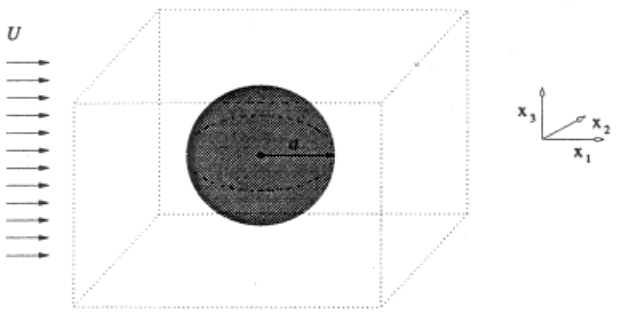

Figure 2. Flow through a periodic array of spheres. The unit cell has periodic boundary conditions on all faces; hence, the sphere in the unit cell experiences a flow that is consistent with an infinite medium of equi-spaced spheres of radius a.

2.2. *Poiseuille flow over a stationary spherical object*

Finally, the forces and torques determined using the LB method for a stationary spherical obstacle placed at various heights in the flow field are benchmarked against the results of Wakiya [3] given in Happel and Brenner [8]. Wakiya used Faxen's [7] approach to calculate the force and torque acting on a stationary sphere held fixed at a vertical position a quarter the way up from the lower bounding wall, i.e., $x_3 = H/4$ (see Figure 3).

Based on this configuration for an isolated sphere, the force in the x_1-direction as reported by Happel and Brenner [8] is

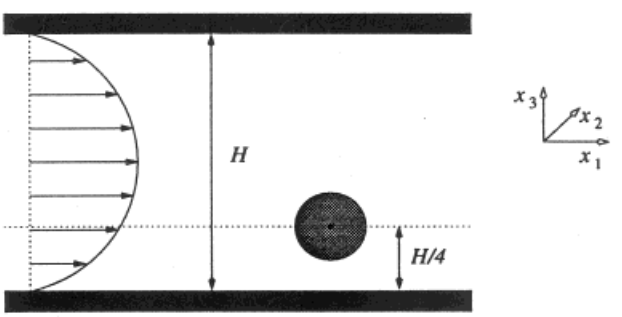

Figure 3. Poiseuille flow over a stationary spherical particle. The unit cell has periodic boundary conditions the x_1- and x_2-directions; hence, the bounded sphere sees infinite parallel plates and periodic images of itself in the x_1–x_2 plane.

$$F_1 = 6\pi\mu a U_\ell \left\{ \frac{1 - \frac{1}{9}\left(\frac{a}{\ell}\right)^2}{1 - 0.6526\left(\frac{a}{\ell}\right) + 0.3160\left(\frac{a}{\ell}\right)^3 - 0.242\left(\frac{a}{\ell}\right)^4} \right\} \tag{2}$$

Here, a is the sphere radius, U_ℓ is the fluid velocity at the $H/4$ position for this same flow configuration without the sphere (see Figure 1), and ℓ is equal to $H/4$. Furthermore, if the sphere is not permitted to rotate, the torque acting on a sphere centered at $H/4$ is

$$T^2 = \frac{8}{3}\pi\mu a^2 U_\ell \frac{a}{\ell}\left[1 + 0.0758\left(\frac{a}{\ell}\right) + 0.049\left(\frac{a}{l}\right)^2\right] \tag{3}$$

Here, T_2 is the torque acting in the x_2-direction. Again, U_ℓ, ℓ, μ, and a are as before.

3. THE LATTICE BOLTZMANN METHOD

The LB method has been described in detail by Chen and Doolen [9] and Ladd [10,11]. Here we present a brief description of the LB method and how it is applied to the problem of interest. For details, the interested reader is directed toward the cited works.

Here we use the 15-bit or 15-lattice velocity model [9,12] to account for the fluid phase, and to calculate the force and torque acting on a stationary spherical particle, we used Ladd's [10,11] half link approach. The fluid parameters are calculated in the usual way. More specifically, the fluid properties of interest, i.e., density and velocity, are determined from the zeroth and *first* moments respectively of the single-particle velocity distribution function $\mathbf{f}(\mathbf{v}, \mathbf{x}, \mathbf{t})$ [16]. Here, $\mathbf{v}$ is the local fluid velocity, $\mathbf{x}$ is the global position, and $\mathbf{t}$ is time. In the LB method, the single-particle velocity distribution function, $\mathbf{f}$, is discretized in velocity, space, and time. When discretizing the velocity, the single particle velocity distribution function takes on a discrete form, i.e., $\mathbf{f}_i(\mathbf{x}, \mathbf{t})$ where i represents the ith lattice velocity $\mathbf{e}_i$.

By applying this discretization and using the single relaxation time BGK collision operator [17], the lattice Boltzmann equation (LBE) has the following form:

$$\mathbf{f}_i(\mathbf{x} + \mathbf{e}_i\Delta\mathbf{t},\ \mathbf{t} + \Delta\mathbf{t}) = \mathbf{f}_i(\mathbf{x}, \mathbf{t}) - \frac{\mathbf{f}_i(\mathbf{x}, \mathbf{t}) - \mathbf{f}_i^{\mathrm{eq}}(\mathbf{x}, \mathbf{t})}{\tau} \tag{4}$$

Here, τ is relaxation time, which is proportional to the fluid viscosity, and $\mathbf{f}_i^{\mathrm{eq}}(\mathbf{x}, \mathbf{t})$ is the equilibrium distribution. The functionality of the equilibrium distribution function is chosen to ensure that both mass and momentum are conserved [9,10].

As mentioned above, the local fluid density is determined by taking a discrete form of the zeroth moment of $\mathbf{f}_i$ or by summing over all of the i components of $\mathbf{f}_i$ locally at each lattice site in the system. Hence, in discrete form

$$\rho = \sum_{i=0}^{n} \mathbf{f}_i(\mathbf{x}, \mathbf{t}) \tag{5}$$

Here, ρ is the local fluid density and n is the number of lattice velocities. The 0 is the *rest* particle or zero velocity contribution to the single-particle velocity distribution function. The momentum density is found from the *first* moment in $\mathbf{f}_i$ with respect to the velocity and is given by the following sum:

$$\rho \mathbf{v} = \sum_{i=0}^{n} \mathbf{f}_i(\mathbf{x}, \mathbf{t})\mathbf{e}_i \tag{6}$$

The local fluid velocity is found by simply dividing Equation (6) by the local density, Equation (5).

To induce a pressure gradient, we add and subtract a *body* force, g, as suggested by Ladd [11], to all of the lattice sites in the system in the desired direction. Therefore, the pressure gradient, g, which represents a vector quantity, must be summed with the appropriate components, i, of the single-particle velocity distribution function, $\mathbf{f}_i$, at each lattice site, i.e., $\mathbf{f}_i = \mathbf{f}_i + e_i g_i$ [15]. For the work presented here, we use the 15-lattice speed model. Consequently, to effect a pressure gradient in the x_1-direction, g is applied to ten components of $\mathbf{f}_i$.

The error in the LB method relative to Equation (1) incurred at the lattice site closest to the bounding wall for the Poiseuille flow configuration shown above in Figure 1, also see Figure 4 below, is quantified in Section 4.

Shown in Figure 4 is a single vertical column of lattice sites that span the gap, H, between the infinite parallel plates. Here the surface of the solid boundary is realized at the halfway position between the wall nodes and the first nodes in the flow field. Because the error between the LB method and theory is greatest at these positions, the relative difference between the LB method and Equation (1) is quantified there. It has been shown by He and Lou [15] that when the no-slip boundary condition is chosen at this halfway position, that the LB method is second-order accurate for this particular flow configuration. In their analysis, however, they normalize the absolute error by the centerline fluid velocity in the channel. Here, we normalize by Equation (1) evaluated at the position in question. As will be shown later in Section 4, our error shows a linear dependence on grid refinement.

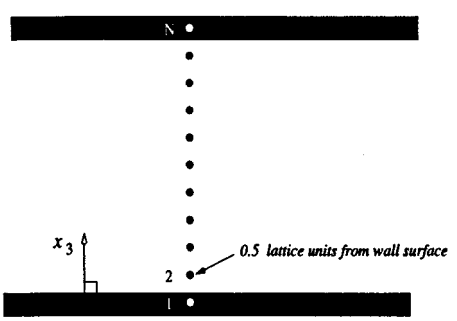

Figure 4. Lattice positions relative to bounding wall. The 1st and Nth lattice sites reside in the bottom and top walls respectively. The 2nd and Nth $-$ 1 lattice sites reside $\Delta x_3/2$ from a wall surface in the fluid.

To calculate the force and torque acting on the stationary particle depicted in Figure 3, we use Ladd's [10,11] half link method. Specifically, the force acting on the stationary body is calculated by considering the local interactions the fluid has with the solid body surface along linking directions, or

$$f_j^{\alpha} = 2[\mathbf{f}_i(\mathbf{x}, \mathbf{t}) - \mathbf{f}_{i'}(\mathbf{x}, \mathbf{t})]\mathbf{e}_i \tag{7}$$

Here, f_j^{α} is the local force acting on particle α at the jth boundary node. The term on the right-hand side is the the first moment with respect to velocity, e_i, of the difference between the ith component of $\mathbf{f}$ crossing from the fluid into the particle and the associated i, where $e_{i'} = -e_i$ is a component of the distribution, $\mathbf{f}$, coming from the particle to the fluid evaluated at the *half*way position between the two lattice sites involved. The total hydrodynamic force acting on the solid body is the sum of the local contributions at the *half* link positions, or

$$F^{\alpha} = \sum_{j=0}^{nb} f_j^{\alpha} \tag{8}$$

where nb is the total number of boundary nodes that represent the surface of the solid body.

The torque on particle α is simply the sum of the vector product of the position vector relative to the particle centroid, which locates each boundary node with the force the fluid exerts on the particle at that same position, or

$$T^{\alpha} = \sum_{j=1}^{nb} \mathbf{r}_j \times f_j^{\alpha} \tag{9}$$

Here T^{α} is the torque acting on particle α. j is the jth boundary node, and nb is the total number of boundary nodes. Finally, $\mathbf{r}_j$ is the position vector locating the boundary node relative to the centroid of the solid body.

To account for solid boundaries, we use the simple bounce back scheme. He and Lou [15] rigorously show that the bounce back scheme achieves better than first-order accuracy when the position of the boundary is taken to be at the half position along lattice links that represent the transition from solid to liquid phase.

For the simulations to follow, $\tau = 1$, and a fluid density, ρ equal to 2 is used. These fluid properties yield a kinematic viscosity, ν, of $\frac{1}{6}$ and a fluid viscosity, μ, of $\frac{1}{3}$ according to $\nu = (2\tau - 1)/6$. A body force is used to effect the pressure gradient that is sufficiently small to ensure Stokes flow, $g = 10^{-9}$ (the Reynolds numbers vary between 0.0001 and 0.00003). The pressure gradient chosen corresponds to a Reynolds number that is much less than one, and the lattice spacing was chosen to ensure that the lattice space Knudsen number, $\Delta x/L$, is also much less than 1. Additionally, all lines through the data to be presented are provided to guide the eye.

4. RESULTS: FUNDAMENTAL FLOW CONFIGURATIONS

In this section, LB simulation results are compared with existing theory and with well-accepted numerical results for the flow configurations cited in Section 2. Specifically, the velocity profile for pressure-driven flow between infinite parallel plates is calculated using the LB method and compared with exact theory, see Equation (1), and the force acting on a periodic array of spheres is determined for various solids fractions and compared with Zick and Homsy [1].

4.1. Poiseuille flow

LB simulations were performed to study pressure-driven flow between infinite parallel plates (Figure 1). To effect the desired pressure gradient, the appropriate body force is applied to each lattice site in the flow field using the approach described in Section 2. The simulations were run to steady state, and the resulting fluid velocities at the first lattice site in the flow field, the 2nd, or the $N\text{th}-1$ lattice sites (Figure 4), are compared with exact theory. The maximum error between the LB method and the analytic solution occurs at these positions. At all other positions in the flow field, there is nearly exact agreement between the LB method and the analytic solution given in Equation (1).

The maximum relative error for the flow configuration shown in Figure 1 varies between 2.82 and 0.23 per cent depending on the lattice site density. The maximum error between the LB method and exact theory for various node densities and for the two approaches used to apply the pressure gradient, are shown in Figure 5.

The relative maximum error, as shown here, varies linearly with increasing numbers of lattice sites. Additionally, the error in the predicted velocity drops below 1 per cent for a node

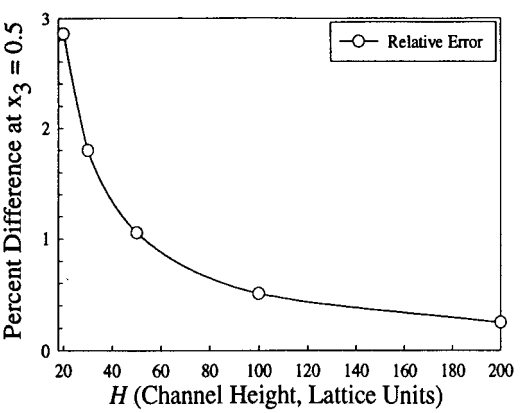

Figure 5. Error near the solid boundary. The maximum error between LB results and the exact solution, see Equation (1), for pressure-driven flow between infinite, parallel plates is compared for various node densities across the height, H, of the flow cell (Figure 4). The separation between the parallel plates, H, ranges from 20 to 200 lattice sites. The $x_3 = 0.5$ position in Figure 4 corresponds to the first lattice site away from the lower wall surface.

density of approximately 55 lattice sites. While this fundamental flow configuration has been examined by others [9,10], it is useful for developing some intuition into the error associated with the simulations to follow.

4.2. Three-dimensional periodic array of spheres

Here the hydrodynamic force acting on a periodic array of spheres (Figure 2) calculated using the LB method is compared with the result of Zick and Homsy [1]. Zick and Homsy [1] used singularity methods based on the Stokes propagator to calculate the force acting on a sphere in a periodic simulation cell. For this particular flow configuration, the LB result is benchmarked with their result to demonstrate that the LB method used here accurately determines hydrodynamic forces over a wide range of solids fractions. The comparison is shown in Figure 6.

The LB results exhibit excellent agreement over the entire range of solids fractions, ϕ, considered.

5. BI-PERIODIC SPHERE BOUNDED BETWEEN PARALLEL PLATES

Here we are interested in calculating the hydrodynamic force and torque acting on a sphere held stationary in Poiseuille flow (Figure 3). For this particular flow configuration, the force and torque were calculated using the LB methods for a sphere held fixed one quarter the way across the vertical gap, $H/4$. The LB results are compared with the theoretical results of Wakiya [3] or Equations (2) and (3) respectively.

To study the effects of periodicity, the size of the simulation cell is varied in the x_1- and x_2-directions at fixed height, H. This is followed by a study of the force and torque on a

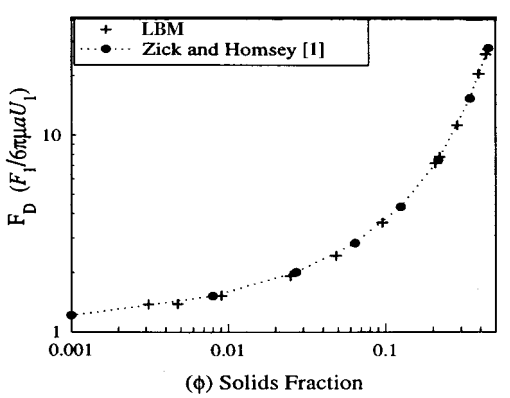

Figure 6. Periodic array of spheres. Lattice Boltzmann simulation results for a periodic array of spheres is compared with the results of Zick and Homsy [1]. The sphere radii range from 5.5 to 54.5 lattice units depending on solids fraction, ϕ. The line through the data is provided to guide the eye.

stationary sphere positioned at various heights in the flow cell of fixed dimensions and for a sphere at fixed height while varying the vertical gap, H, between the bounding walls.

To compare with Wakiya, see Equations (2) and (3), a sphere radius of 5.5 lattice sites is held fixed at the quarter vertical position in a simulation cell, where $H = 50$ lattice units. The bi-periodic directions, x_1 and x_2, are varied until the test sphere is effectively decoupled hydrodynamically from its periodic neighbors. A depiction of the flow configuration, which includes the nearest in-plane periodic images, is shown in Figure 7.

Figure 7 shows a single sphere in flanked by its periodic images in the x_1–x_2 plane. The images that extend into and out of the page, which are not shown, are also a distance D from the central sphere. As discussed in Section 4, we are interested in calculating the hydrodynamic force and torque acting on the central sphere.

Shown in Figure 8 is the force the fluid exerts on the sphere as a function of flow cell size in the x_1–x_2 plane or distance between periodic images.

In Figure 8 the force calculated from the LB method and Equation (2) is made dimensionless with Stocks drag force, where U_ℓ is the fluid velocity form Equation (1) evaluated at $H/4$. Additionally, the center-to-center distance between the test sphere and its periodic images, D, is made dimensionless with the sphere radius, a. The hydrodynamic force increases with increasing separation between periodic images. This is consistent with what Dabros and van de Ven [4] observed for two aligned stationary spheres in a simple flow field directed along the line of centers.

Another observation is that for an infinite medium of periodic spheres [1], the hydrodynamic force acting on the test sphere decreases with decreasing solids fraction (Figure 5). In contrast, the force for the case shown in Figure 8, the hydrodynamic force increases with decreasing solids fraction. This is due to the fact that for the case of the infinite medium of periodic spheres, the flux area for fluid decreases with increasing solidities, and for a constant pressure gradient this results in an increase in drag force. In contrast to the case studied here, the flux area for fluid is a constant and the periodic images tend to shield the test sphere less and less

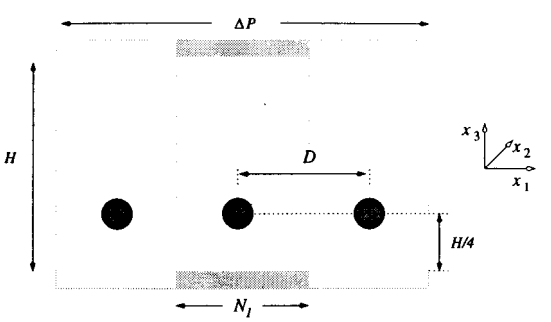

Figure 7. Bi-periodic bounded flow cell. A test sphere of radius a at a height of $H/4$ is in the central flow cell, which has vertical gap between the bounding walls of H with a length of N_1 ($= D$) in the x_1- and x_2-directions. The periodic images in the x_1–x_2 plane are shown to be a distance D away from the central sphere.

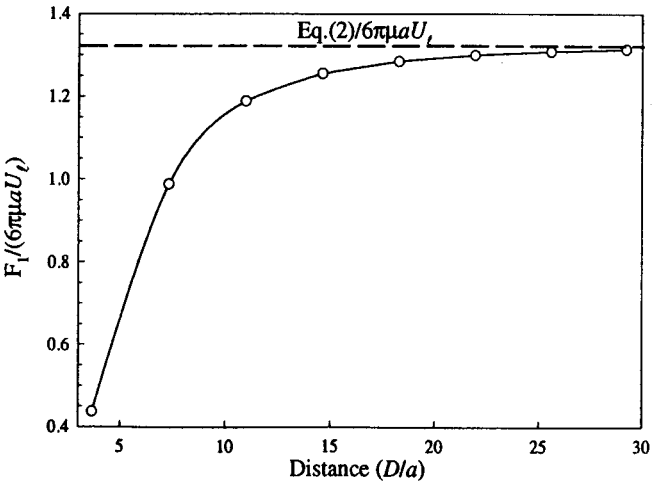

Figure 8. Force acting on a bounded periodic sphere. LB results are compared with the result of Wakiya given in Equation (2). The dimensionless hydrodynamic force in the x_1-direction, F_1, acting on the central sphere in Figure 7 is plotted as a function of the dimensionless, center-to-center distance, D/a, between periodic images. The vertical position of the sphere is fixed at $H/4$. U_ℓ is the fluid velocity from Equation (1) evaluated at $H/4$.

as D is increased; hence, at large D the test sphere feels the full impact of the flow field, i.e., the incident flow has time to recover from disturbances caused by neighboring periodic images. Naturally, the torque exhibits similar behavior in magnitude as a function of the distance between periodic images, D, see Figure 9.

Here the torque in the x_2-direction calculated from the LB method and from Equation (3) is made dimensionless with the torque acting on an isolated sphere rotating with an angular velocity of U_ℓ/ℓ. Again, U_ℓ is the fluid velocity calculated by Equation (1) evaluated at $x_3 = H/4$. As expected, the torque converges to the desired solution expected for an isolated sphere when center-to-center separation between the test sphere and its periodic images, D/a, is greater than or equal to 30.

Additionally, LB studies are performed to facilitate estimates for forces and torques acting on a fixed sphere for variations on the flow configuration used in Figure 7. Specifically, the vertical position of the sphere is varied while holding the flow cell dimensions fixed, and the magnitude of the vertical gap between the bounding walls, H, is varied while holding the sphere at a fixed vertical position and holding the x_1 and x_2 dimensions of the flow cell fixed.

5.1. Results: variable height

In the presence of external fields, it is possible that a particle could be captured and drawn to either the lower or upper surface via an induced force. As a consequence, it is important to know the hydrodynamic force and torque acting on a stationary sphere at various vertical positions in the flow cell. Shown in Figure 10 are LB results for a sphere held fixed at various vertical positions in a bi-periodic simulation cell of fixed dimensions.

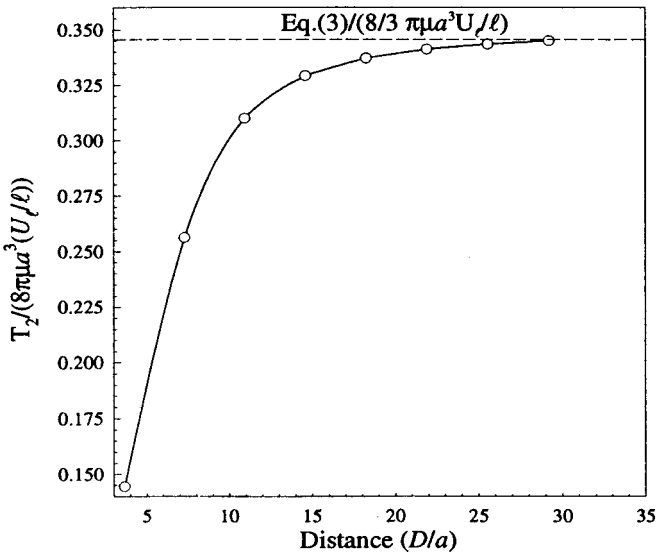

Figure 9. Torque on a bounded periodic sphere. LB results are compared with the result of Wakiya [3] given in Equation (3). The dimensionless hydrodynamic torque in the x_2-direction, T_2, acting on the central sphere in Figure 7 is plotted as a function of the dimensionless, center-to-center distance, D/a, between periodic images. The vertical position of the sphere is fixed at $H/4$. U_ℓ is the fluid velocity from Equation (1) evaluated at $H/4$. Here, ℓ is equal to $H/4$.

The bi-periodic simulation cell is 110 lattice sites in both the x_1- and x_2-directions. The simulation cell height, H, is equal to 94 lattice sites, and the sphere radius is 5.5 lattice sites; hence, the dimensionless lengths of the simulation cell in the x_1- and x_2-directions, corresponding to Figure 7, are held fixed at 20. The force is made dimensionless using Stokes drag force, where U_ℓ is the fluid velocity calculated using Equation (1) evaluated at $x_3 = H/4$. The x_3 component of the sphere origin is made dimensionless with the channel height H.

The results above are for heights, x_3, of a, the sphere radius, $H/8$, $H/4$, $3H/8$, and $H/2$. As a consequence, the force response shown above begins at a finite value. As shown, the force increases monotonically as the sphere is moved toward the mid-plane of the flow cell. This is consistent with the increase in fluid velocity as one moves toward the mid-plane of the flow cell; hence, the force is a minimum at the wall and a maximum at $x_3 = H/2$.

The torque on the stationary sphere exhibits the opposite behavior; namely, the torque is at a maximum when the sphere is resting on the wall surface and a goes to zero at the mid-plane of the flow cell, see Figure 11.

The torque results from an uneven distribution of force acting on the sphere surface. In our flow cell, the undisturbed velocity profile is parabolic, and the distribution of force acting on the stationary sphere is directly proportional to the imposed fluid velocity impinging on the sphere surface. The interesting feature in the torque response occurs near the mid-plane of the flow cell. Specifically, there is a *slight* inflection point in the above curve when the center of

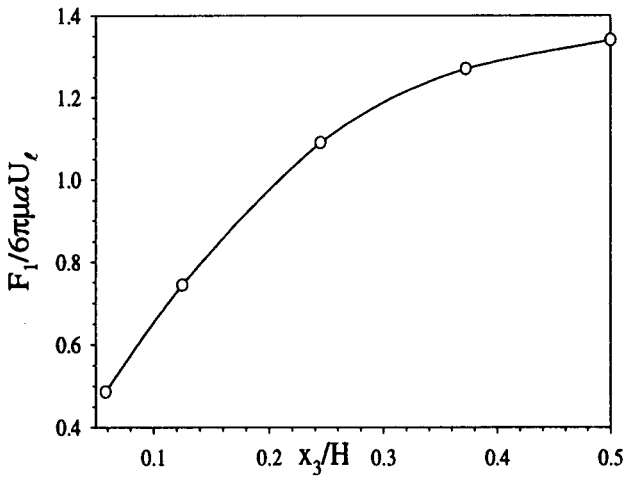

Figure 10. Force on a bounded, periodic sphere as a function of vertical position. The dimensionless force acting on a sphere in the bi-periodic flow cell shown in Figure 8 is plotted as a function of dimensionless vertical position. The sphere radius is 5.5 lattice sites and the dimensions of the simulation cell are $110 \times 110 \times 94$ for the x_1-, x_2-, and x_3-directions respectively. U_ℓ is the fluid velocity calculated at $x_3 = H/4$ using Equation (1). The vertical position of the sphere origin is made dimensionless by the vertical gap between the bounding walls, H, in the flow cell.

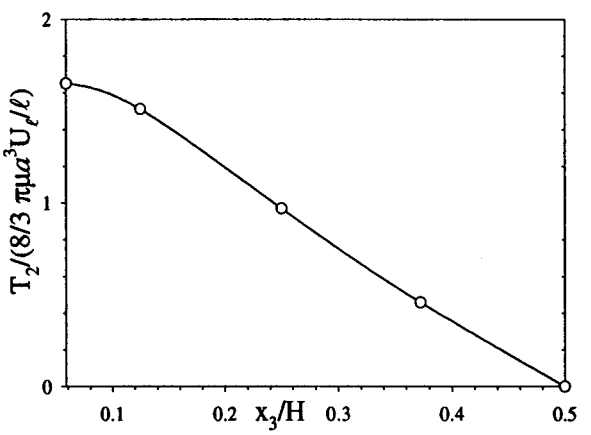

Figure 11. Torque on a bounded, periodic sphere as a function of vertical position. The dimensionless torque acting on a sphere in a bi-periodic flow cell is plot as function of dimensionless vertical position. The sphere radius is 5.5 lattice sites and the x_1 and x_2 dimensions of the simulation cell are both 110 lattice sites. The vertical gap between the bounding walls, H, is 94 lattice sites. U_ℓ is the fluid velocity calculated at x_3 or $\ell = H/4$ using Equation (1).

the particle is near $x_3 = H/8$ in the simulation cell. This is possibly due to the fact that the test sphere is within 30 sphere radii of its upstream and downstream periodic images. As a result, the calculated forces and torques are reduced due to the drafting effect (Figures 8 and 9). However, at all separations, D, between periodic images, the resulting trends all pass through zero at the mid-plane, i.e., $x_3 = H/2$. Therefore, for $D < 30$, the trends are expected to exhibit an inflection points near the mid-plane. Estimates for forces and torques at various separations and heights can be made using the results presented in Figures 10 and 11 together with the results in Figures 8 and 9.

To explore the effects of changing H, which is equivalent to changing the radius of the test sphere while using a fixed H, simulations are performed with three different flow cell heights while holding the sphere radius and absolute position fixed, see Figure 12.

The force shown in Figure 12 has been made dimensionless with Stokes drag using the fluid velocity for the associated flow cell evaluated at $x_3 = H/4$ using Equation (1). Additionally, the vertical gap between bounding walls, H, has been made dimensionless with the sphere radius, a. The sphere is held fixed at a vertical position of 12.5 lattice sites. For the simulation cell of $H = 50$, this represents the quarter position.

As shown above, the force decreases as the vertical gap is increased. As the vertical gap, H, is increase, the sphere samples a reduced fluid velocity, i.e., the relative position of the sphere in the simulation cell approaches the wall as H is increased. As a result, the *dimensionless* force decreases with increasing H. Also, the difference in the force response is reduced as the relative difference between the vertical gap, H, and the fixed position of the sphere position, 12.5 lattice units, becomes large.

The associated torque shown in Figure 13 for this flow system exhibits the expected opposite trend.

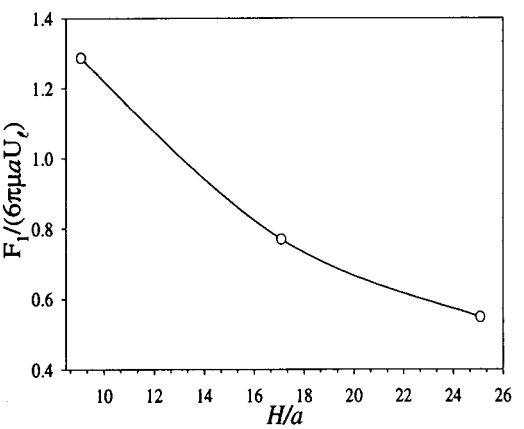

Figure 12. Force on a bounded, periodic sphere as a function of the vertical gap between bounding walls, H. The sphere radius is 5.5 lattice sites, and the simulation cell lengths in both the x_1- and x_2-directions is held fixed at 110 lattice sites. $H = 50$, 94 and 138 lattice sites. U_f is the fluid velocity calculated at $x_3 = H/4$ using Equation (1) for each H used.

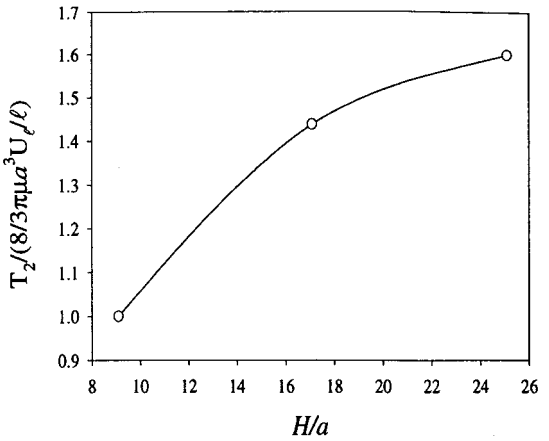

Figure 13. Torque on a bounded, periodic sphere as a function of the vertical gap, between bounding walls, H. The sphere radius is 5.5 lattice sites, and the simulation cell lengths in both the x_1- and x_2-directions is held fixed at 110 lattice sites. $H = 50$, 94 and 138 lattice sites. U_ℓ is the fluid velocity calculated at $x_3 = H/4$ using Equation (1) for each H.

All terms used here are as before. Analogous to the force response shown above, the torque initially increases rapidly with increasing H, but when H is much larger than the fixed particle position, the torque response becomes increasingly similar in magnitude. As H is increased, the relative position of the sphere decreases below $H/4$ and the torque response increases (see Figure 11).

If the force and torque where made dimensionless by a constant, say, U_ℓ for $H = 50$, the force and torque responses decrease and increase linearly with increasing H respectively over the interval of H explored. It is not intuitively obvious why this is the case, since the incident fluid velocity profile is quadratic in x_3. This is due to the fact that the gradient in the fluid velocity changes in a near linear fashion at the chosen particle height for range of H presented. The results presented in Figures 12 and 13 can be combined with previous results to predict the force and torque acting on a test sphere at various heights and separations, D, for various channel gaps, H.

6. CONCLUSIONS

For pressure-driven flow between parallel plates, numerical results show a linear reduction in the relative error, as calculated here, in the no-slip condition with grid refinement. LB results for flow through an infinite medium of spheres are in excellent agreement with Zick and Homsy [1]. While this result is not new [10,11], it serves as a fundamental verification of the LB approach used here, and it demonstrates that the LB method used is accurate for a wide range of solids fractions. LB results for pressure-driven flow over a sphere held fixed at $H/4$

in a bi-periodic flow cell exhibit a good agreement with the theory of Wakiya [3]. Studies of the force and torque on the sphere as a function of distance between periodic images reveal a *drafting*-like phenomenon, which reduces both the force and torque acting on the test sphere. It was found that the distance between images needs to be ≥ 30 sphere radii to ensure that the test sphere is hydrodynamically decoupled from its neighboring periodic images. The slight inflection in the torque response shown in Figure 11 gives evidence that it arises from the drafting phenomenon coupled with the fact that all torque trends will pass through zero at the mid-plane regardless of the separation between periodic images. Finally, the results show that the force and restraining torque necessary to hold a particle in a stationary, captured state, e.g., via external electric fields, is very much dependent on the proximity of neighboring captured particles.

ACKNOWLEDGMENTS

This research was conducted under the auspices of the U.S. Department of Energy by Lawrence Livermore National Laboratory, contract number W-7405-ENG-48. The authors would also like to thank the Lawrence Livermore computing facilities for computational time. In particular, the calculations performed for the revision of this paper were performed on the LLNL Tera Cluster. Finally, D Clague would like to thank the Center for Computational Engineering for financially sponsoring this work.

REFERENCES

1. Zick AA, Homsy GM. Stokes flow through periodic arrays of spheres. *Journal of Fluid Mechanics* 1982; **115**: 13–26.
2. Probstien RF. *Physicochemical Hydrodynamics. An Introduction*. Wiley: New York, 1994.
3. Wakiya S. *Journal of the Physical Society of Japan* 1957; **12**: 1130–1141.
4. Dabros T, van de Ven TGM. Hydrodynamic interactions between two spheres near a solid plane. *Journal of Multiphase Flow* 1992; **18**(5): 751–1992.
5. Durlofsky LJ, Brady JF. Dynamic simulation of bounded suspensions of hydrodynamically interacting particles. *Journal of Fluid Mechanics* 1989; **200**: 39–67.
6. Hu HH. Direct simulation of flows of solid-liquid mixtures. *International Journal for Multiphase Flow* 1996; **22**(2): 335–352.
7. Faxen H. Der Widerstand gegan die bewegung einer starren Kugel in einer zähen Flüssigkeit, die zwischen zwei parallelen, ebenen Wänden eingeschlossen ist. *Arkiv Matematik Astronomi och Fysik* 1924; **18**(29): 1–52.
8. Happed J, Brenner H. *Low Reynolds Number Hydrodynamics*. Kluwer Academic: Dordrecht, 1991.
9. Chen S, Doolen GD. Lattice Boltzmann method for fluid flows. *Annual Review of Fluid Mechanics* 1998; **30**: 329–364.
10. Ladd AJC. Numerical simulations of particulate suspensions via a discretized Boltzmann equation. Part 1. Theoretical foundation. *Journal of Fluid Mechanics* 1994; **271**: 285–309.
11. Ladd AJC. Numerical simulation of particulate suspensions via a discretized Boltzmann equation. Part 2. Numerical results. *Journal of Fluid Mechanics* 1994; **271**: 311–339.
12. Clague DS, Kandhai BD, Zhang R, Sloot PMA. The hydraulic permeability of (un)bounded fibrous media. *Physical Review E* 2000; **61**(1): 616–625.
13. Aidun CK, Lu YN, Ding EJ. Direct analysis of particulate suspensions with inertia using the discrete Boltzmann equation. *Journal of Fluid Mechanics* 1998; **373**: 287–311.
14. Zou Q, He X. On pressure and velocity boundary conditions for the lattice Boltzmann BGK model. *Physics and Fluids* 1997; **9**(6): 1591–1598.
15. He X, Luo L. A priori derivation of the lattice Boltzmann equation. *Physical Review E* 1997; **55**(6): R6333–R6339.
16. Lifshitz EM, Pitaevskii LP. In *Course in Theoretical Physics*, vol. 10, Landau, Lifshitz (eds). Pergamon Press: Oxford, 1989; 1–16.
17. Martinez D, Chen S, Chen H, Matthaeus WH. Lattice Boltzmann model for simulating magnetohydrodynamics. *Physics Review Letters* 1991; **67**: 3776–3779.

